analytical chemistry

Article

Cite This: *Anal. Chem.* 2020, 92, 1738−1745

pubs.acs.org/ac

Gating a Single Cell: A Label-Free and Real-Time Measurement Method for Cellular Progression

Saw Lin Oo,[†] Shishir Venkatesh,[†] Abdul-Mojeed Ilyas,[†] Vaithinathan Karthikeyan,[†] Clement Manohar Arava,[†] Eva Yi Kong,[‡] Chi-Chung Yeung,[§] Xianfeng Chen,[∥] Peter K. N. Yu,*[,‡] and Vellaisamy A. L. Roy*[,⊥]

[†]State Key Laboratory for THz and Millimeter Waves and Department of Material Science and Engineering, City University of Hong Kong, Kowloon, Hong Kong, S.A.R.

[‡]Department of Physics, City University of Hong Kong, Kowloon, Hong Kong, S.A.R.

[§]Department of Chemistry, City University of Hong Kong, Kowloon, Hong Kong, S.A.R.

[∥]School of Engineering, Institute for Bioengineering, The University of Edinburgh, King's Buildings, Mayfield Road, Edinburgh EH9 3JL, United Kingdom

[⊥]James Watt School of Engineering, University of Glasgow, Glasgow G12 8QQ, United Kingdom

Supporting Information

ABSTRACT: There is an ever-growing need for more advanced methods to study the response of cancer cells to new therapies. To determine cancer cells' response from a cell-mortality perspective to various cancer therapies, we report a label-free and real time method to monitor the in situ response of individual HeLa cells using a single cell gated transistor (SCGT). As a cell undergoes apoptotic cell death, it experiences changes in morphology and ion concentrations. This change is well in line with the threshold voltage of the SCGT, which has been verified by correlating the data with the cell morphologies by scanning electron microscopy and the ion-concentration analysis by inductively-coupled plasma mass spectrometry (ICPMS). This SCGT could replace patch clamps to study single cell activity via direct measurement in real time. Importantly, this SCGT can be used to study the electrical response of a single cell to stimuli that leaves the membrane intact.

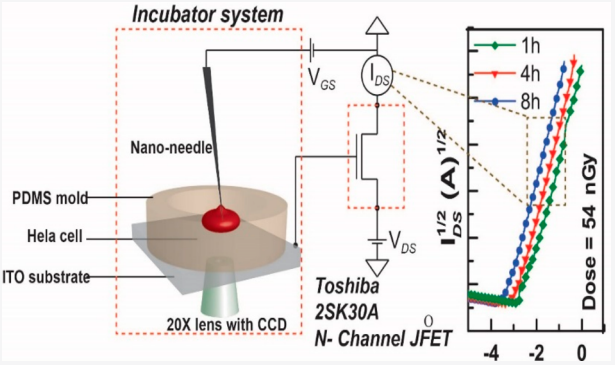

Multiparameter models from different perspectives are required to understand the noisy and complex responses of single cancer cells to various stimuli. Single cell technology is essentially required for resolving cancer heterogeneity with distinct morphological and phenotypic profiles for individual cells.[1] Single cell technologies can be classified into single cell separation and single cell analysis. Single cell separation is the basis of cell analysis which provides data of cell's genomic, transcriptomic, and proteomic profiles[2] through methods like optical tweezers, flow cytometry, microfluidics, and laser capture microdissection (LCM). These approaches have the advantage of averaging out the cellular responses and information, but with an important disadvantage of not covering up the presence of cellular functional subpopulations. Normally, cancer cell death occurs through changes in cell morphology, destruction of ion concentration equilibrium and development of apoptosis bodies followed by cell rupturing.[3] Observation of single cells undergoing apoptosis in real time can provide insights into the metabolic pathways and facilitates to build a conceptual understanding of the whole process. The real time and in situ measurements can help to comprehensively track the changes occurring in live cancer cells over the entire duration of an experiment. Particularly, studying their ion channel activity makes it possible to track the development of apoptotic stages as it provides deep insights in creating a diagnostic tool on how to detect cancer.[4]

For single cell analysis, fluorescence microscopy is a powerful tool which uses labeling tags for molecules to optically track their ion concentration and estimate membrane potential of the cell.[5] Anionic/cationic fluorescent dyes are used as optical indicators which help to understand both the ion channel change and also the membrane potential.[6] However, fluorescence microscopy requires significant cell sample preparation procedures such as cell fixation and permeabilization, cell components extraction, fluorescent tag labeling, making a real-time and in situ monitoring of responses to ionizing radiation impossible.[7] Additionally, the

Received: July 11, 2019
Accepted: December 20, 2019
Published: January 6, 2020

DOI: 10.1021/acs.analchem.9b03136
Anal. Chem. 2020, 92, 1738−1745

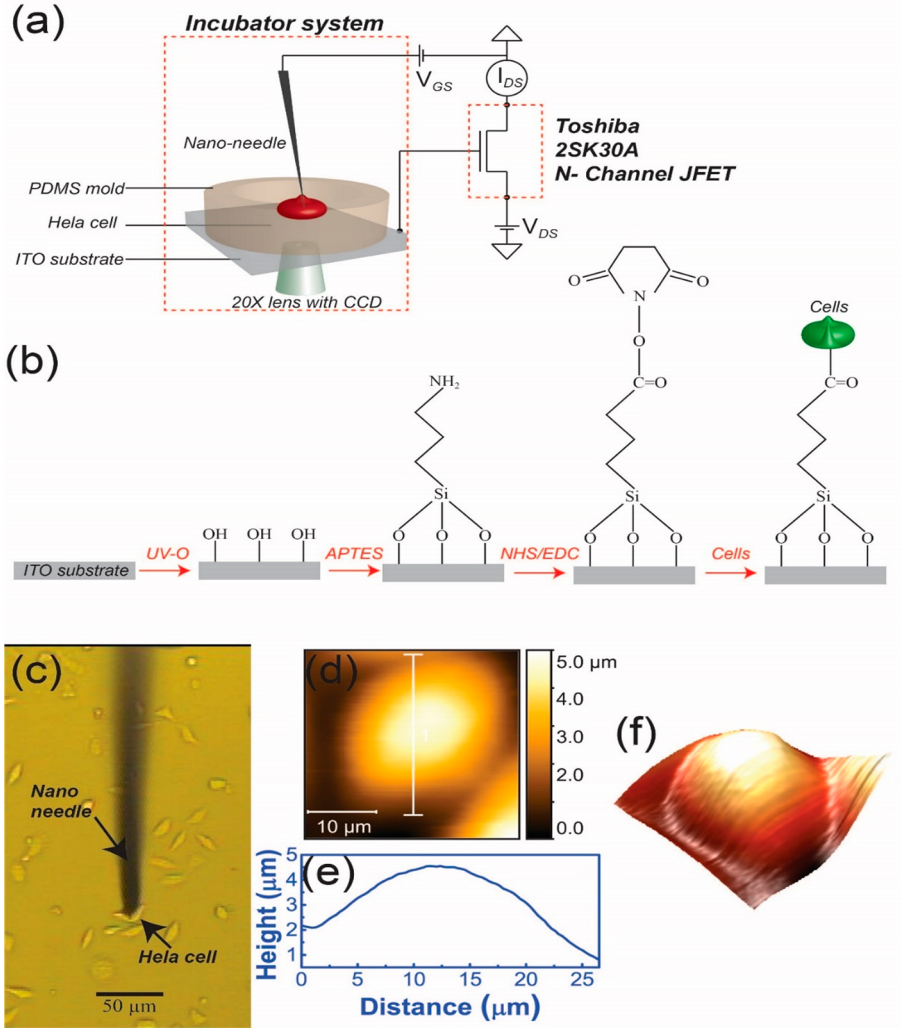

Figure 1. Schematic diagram of the electrical measurement and cell immobilization: (a) transistor based electrical measurement system, (b) cell immobilization process on the ITO electrode, (c) nanoneedle for single-cell electrical measurement, (d) AFM images for single HeLa cells, (e) height and distance graph of the single cells AFM analysis, and (f) AFM 3D images for single HeLa cells.

labeling may affect the normal function of cells and ruin the purpose of the study. While fluorescence microscopy is useful in understanding the dynamics of gene expression and transcription, it does not provide a holistic picture of cells.[8]

Alternatively, electrical measurements of single cells are commonly achieved through whole-cell patch-clamp methods.[9] In this method, the larger opening of the patch-clamp electrode tip affords the lower resistance and thus better electrical access to the inside of the cells. However, this method results in the complete rupture of the cell-membrane, thereby making long-time interval real-time and in situ measurements difficult to achieve.[10] Accompanying fluorescence microscopy with measurement of electrical properties of the cells can provide insights into the cell mechanisms such as ion channels and membrane potential, which are key in explaining cell-fate like cell proliferation, apoptosis, and cell division.[11]

In order to advance the existing methods of single cell analysis, we have developed a new technique to monitor cells in real time and in situ to monitor the important parameters related to general behavior and response to various stimuli at the single cell level. As this proposed method is real-time and in situ, it is possible to track the cell mortality and determine its progress along the apoptotic stages. This knowledge will enable to monitor the diffusion across ion-channels, an indicator of cell death progression, to design and optimize therapeutic treatment options. The central component to this method is single cell gated transistor (SCGT) to measure ion concentration changes,[12] capacitance, and membrane potential changes with a high sensitivity. In our technique, we use a single cell gate approach to physically and electrically insulate the electronic transducer FET from the single cell gate detector in which biological solutions are placed. The single cell gated transistor (SCGT) can be placed inside an incubator environment to monitor the activities of living cells for a prolonged time and does not require labeling agents. As such, the SCGT is a promising method for real-time and in situ analysis of single cells.[13]

To verify our technique, we used the SCGT to study the apoptosis process of single HeLa cells via observing the threshold voltage shifts in real-time under in situ conditions. In addition, the cell morphologies and ion concentrations are recorded with scanning electron microscopy (SEM) and inductively-coupled plasma mass spectrometry (ICPMS), respectively, followed by establishing a correlation of the data with the threshold voltage shifts from the SCGT. Through

DOI: 10.1021/acs.analchem.9b03136
Anal. Chem. 2020, 92, 1738−1745

the study, we found that the shift in threshold voltage clearly reveals the stage of apoptosis and explains the underlying mechanism of cell death process. Overall, we provide a new technology to conveniently determine single cancer cells' responses to various cancer therapies without the need of using expensive equipment and labeling agents.

EXPERIMENTAL SECTION

General Experimental Setup. Single cell measurement was carried out by the experimental setup shown in Figure 1a. Here the ITO-coated glass served as a single cell gate electrode which is connected to the gate terminal of Toshiba 2SK30ATM n-channel JFET. The nanoneedle (Naulga NN-EEUSNP-W500, length 3−5 μm with Parylene "C" coating) was used to pierce through the cell membrane. All electrical characterization was carried out using an Agilent 4155C semiconductor parameter analyzer. The movement of the nanoneedle was controlled using a micromanipulator stage (Thorlabs RBL 13dl/m). Nikon objective lens with working distance of 3.6 mm and magnification of 20× combined with a Sony (SSC-C370P) color video camera was used for live imaging of the HeLa cells and the nanoneedle. An ^{241}Am alpha-particle source with an activity of 5.02 μCi and average energy of 5.16 MeV was used for cell irradiation[14] and irradiation doses of 27, 54, and 81 nGy is systematically experimented. Prior to irradiation of the cells, the cell concentration was determined using the hemocytometer.[15,16] Subsequent changes in the cell's morphology and its ion concentration change according to the irradiation doses applied are deeply analyzed through SEM and ICPMS, respectively.

Materials. Dulbecco's modified Eagle's essential medium (DMEM), fetal bovine serum (FBS), and trypsin and phosphate-buffered saline (PBS) solutions (Gibco Grand Island, NY) were purchased from Thermo Fisher Scientific, Hong Kong, for cell culture and growth. For substrate modification, 3-aminopropyl triethoxysilane (APTES), 1-ethyl-3-[3-dimethy-laminopropyl] carbodiimide hydrochloride (EDC), and *N*-hydroxy-succinimide (NHS) were purchased from Sigma-Aldrich. Sylgard 184 Silicone Elastomer Kit (polydimethylsiloxane) was purchased from Dow Corning.

Cell Culture. HeLa cells obtained from a human epithelial carcinoma cell were grown in Dulbecco's modified Eagle's essential medium (Gibco, Grand Island, NY) with 10% fetal bovine serum (FBS) inside the 5% carbon-dioxide (CO_2) incubator under constant temperature of 37 °C.[17]

Substrate Cleaning. Glass substrates coated with 30 ohm/square, indium tin oxide (ITO) were cut into 1.5 in. squares and cleaned sequentially using 5% Decon 90, ethanol, acetone, and deionized water for 15 min each in bath sonicator, followed by drying with high-purity nitrogen gas.[18]

Preparation of PDMS Well on ITO Substrate. Sylgard 184 Silicone Elastomer Kit was used for making polydimethylsiloxane (PDMS) wells. First, the uncured resin was mixed homogeneously with curing agent in a 10:1 weight ratio.[19,20] Then, the mixture was degassed in vacuum (base pressure, 700 mmHg) to remove bubbles. The clear and homogeneous solutions were poured onto molds to create wells with an inside diameter of 12 mm. PDMS was then cured by baking at 85 °C for about 30 min. The PDMS wells were peeled off from the mold and bonded to the cleaned ITO substrate.[21]

Immobilization of HeLa Cells on ITO Substrate. The ITO substrates with PDMS wells were cleaned with 100% ethanol and DI water. After drying with nitrogen gas, the samples were subjected to UV−ozone treatment (Jelight Company 144AX-220) for 30 min to generate hydroxide bonds on the surface.[18] Treated ITO substrates were incubated in a solution of APTES in methanol (2%) for 30 min to modify the substrates. Then, the modified substrates were treated with a NHS/EDC solution (NHS, 3 mg mL^{-1}; EDC, 2 mg mL^{-1}) for 1 h at ambient temperature[22] and rinsed with 1× PBS buffer solution to remove the unbound/unreacted molecules.[22] NHS/EDC modified substrates were incubated with a suspension of living HeLa cells in DMEM with 10% FBS inside the 5% CO_2 incubator under constant temperature of 37 °C for about 24 h.[23] After incubation, the samples were gently rinsed with copious amount of 1× PBS buffer (<2 mL) to remove the old medium or loosely attached cells. The rinsed samples were kept in growth medium at 37 °C for further analysis.[24] Immobilization process of HeLa cells on ITO substrates are shown in Figure 1b.

Transfer of Cells from Stock Medium to Modified ITO-Coated Glass Substrates. To transfer the cells from the cell culture Petri-dish to ITO coated glass with PDMS wells, first the medium was removed from the cell culture Petri-dish. Subsequently, the cells were washed by 1× PBS to remove dead cells. Then, the cells were released from the Petri-dish by washing with 0.25% trypsin solution for 2 min inside the incubator at 37 °C. Then, trypsin was removed and DMEM with 10% FBS was added to the cell suspension. This suspension was diluted to attain a cell concentration of 3 × 10^4 cells mL^{-1}. This cell suspension was then transferred onto the modified ITO-coated glass. The substrates were subsequently incubated for 24 h. The pH throughout the whole experiment was maintained at 7.4, and all the previous steps were performed in the biosafety fume hood.[25]

Preparation of Unirradiated Cells. The "control" unirradiated cells were also left exposed without medium for 1, 2, and 3 min. However, no radiation was applied to these control unirradiated cells. Then 800 μL of fresh medium was filled into the PDMS wells. Then substrates were subsequently loaded into the incubator for further characterization.

Sample Preparation for Scanning Electron Microscopy. For the SEM analysis, 3 × 10^4 cells on plastic tissue coverslips (Thermanox TMX Coverslips) were fixed in 2.5% glutaraldehyde and 2% paraformaldehyde in PBS solution for 2 h, washed in PBS for five times (100, 100, 100, 50, and 25%) and two times in double deionized water (100%, 100%) for 10 min each.[26] After that, samples were dehydrated with increasing concentration of ethanol (30, 50, 70, 80, 90, 95, 100, and 100%). Subsequently, the samples were immersed in the mixture of ethanol and acetone (3:1, 1:1, 1:3), and three times in 100% acetone for 10 min each. After dehydration, the specimens were critical point dried in liquid CO_2 (BAL-TEC CPD 030 Critical Point Dryer) for about 1 h. Finally, the specimens were mounted on the aluminum stubs and sputter coated with 10% Au using BAL-TAC SCD050 instruments.[27] Images were taken by using Phillips XL30ESEM FEG scanning electron microscope at an accelerating voltage of 10 kV under vacuum (base pressure, 10^{-5} Pa).

Inductively Coupled Plasma Mass Spectrometry (ICPMS). This is a technique for the detection of ion concentration in solution.[28] In this work, Optima 2100 DV ICP-OES system was used for potassium ion (K^+) concentration analysis. Before analysis, 3 × 10^4 cells were cultured on each 10 mL Petri dish for radiation and control measurements.

DOI: 10.1021/acs.analchem.9b03136
Anal. Chem. 2020, 92, 1738−1745

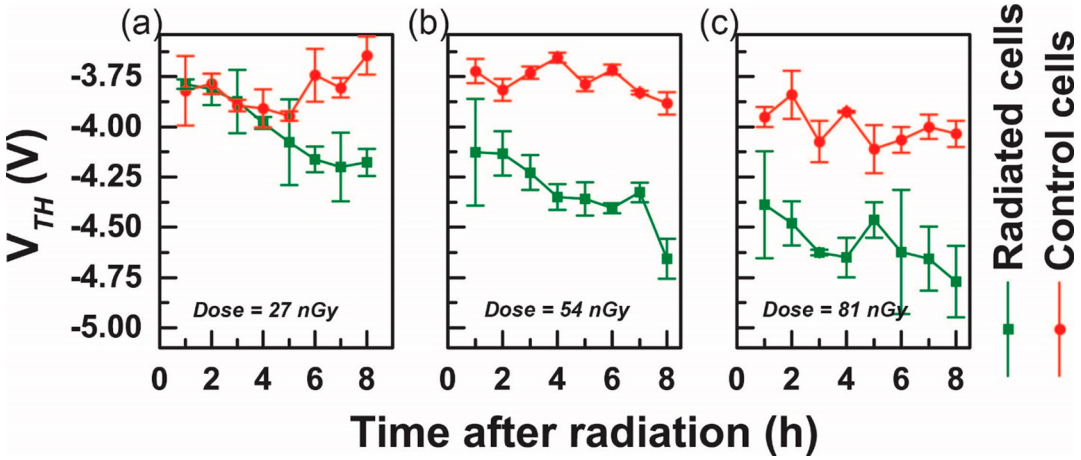

Figure 2. Threshold voltage and time graphs (a) V_{th} and time graph for 27 nGy irradiated cells and control. (b) V_{th} and time graph for 54 nGy irradiated cells and control. (c) V_{th} and time graph for 81 nGy irradiated cells and their control cells. The statistical analysis was performed on data obtained from three different samples.

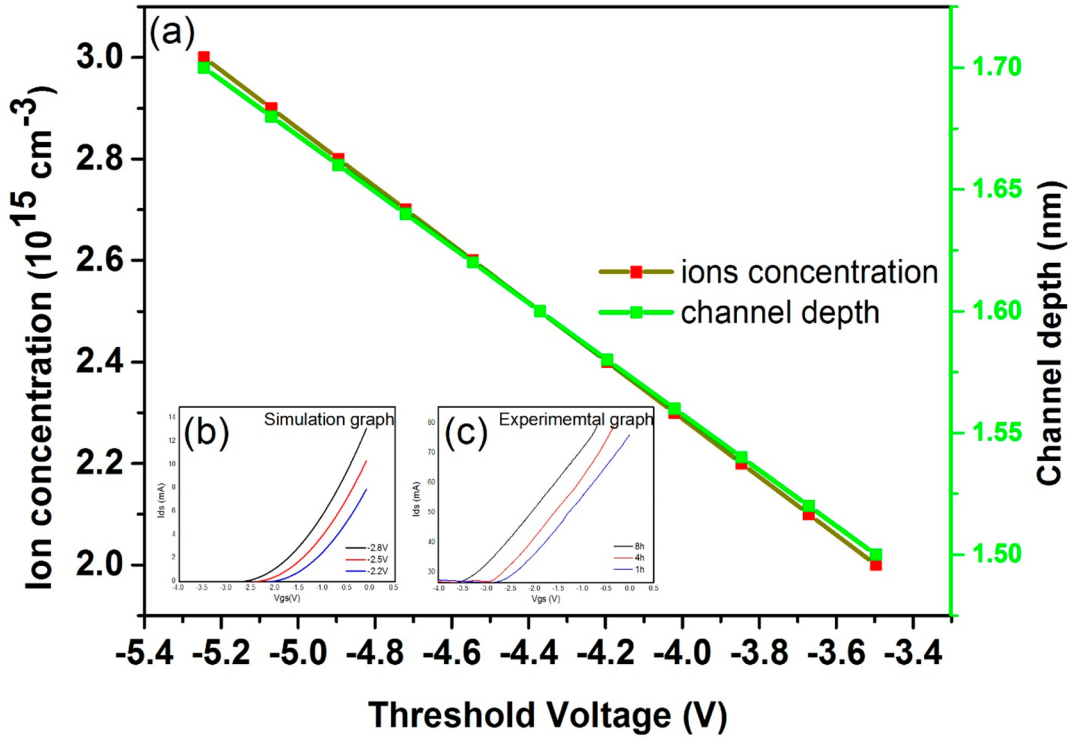

Figure 3. Modeling simulation graph (a) shows the threshold voltage shifts graph with respect to ion concentration and channel width or depth (b) and (c) shows the comparison of experimental and simulated $I-V$ curves.

Samples were kept inside the incubator for 24 h with 5% CO_2 and 37 °C. After 24 h, three samples were used for radiation and another three samples were used for control measurements. Before irradiation, old medium solution was removed and washed with 1× PBS for removing dead cells and other impurities. After being washed with (2 mL) PBS solution, the cells (3×10^4) were irradiated with the ^{241}Am α-particle source for different periods such as 27 nGy, 54 nGy, and 81 nGy. For the control samples, removed the old medium solution from the cell surface, washed with 1× PBS and kept the samples without medium for 1, 2, and 3 min. The medium was collected from both irradiated and control samples for each 1, 4, and 8 h. Finally, the samples were diluted 100 times for potassium ion (K^+) analysis.

RESULTS AND DISCUSSION

Single Cell Electrical Measurements. The real time measurement of single cell is achieved in the SCGT sketched in Figure 1a. In the setup, single cells are first immobilized on an ITO glass substrate via the procedures presented in Figure 1b and then a nanoneedle with a tip diameter of 60 nm will be pierced to a single HeLa cell with a depth of approximately 2.5 μm into the cell membrane with the help of micromanipulator which prevents the nanoneedle and ITO substrate to electrically short. The device design is based on our atomic force microscopy (AFM) measurement of the morphological information on HeLa cells (Figure 1d–f. During the measurement, HeLa cells are first irradiated to induce

DOI: 10.1021/acs.analchem.9b03136
Anal. Chem. 2020, 92, 1738–1745

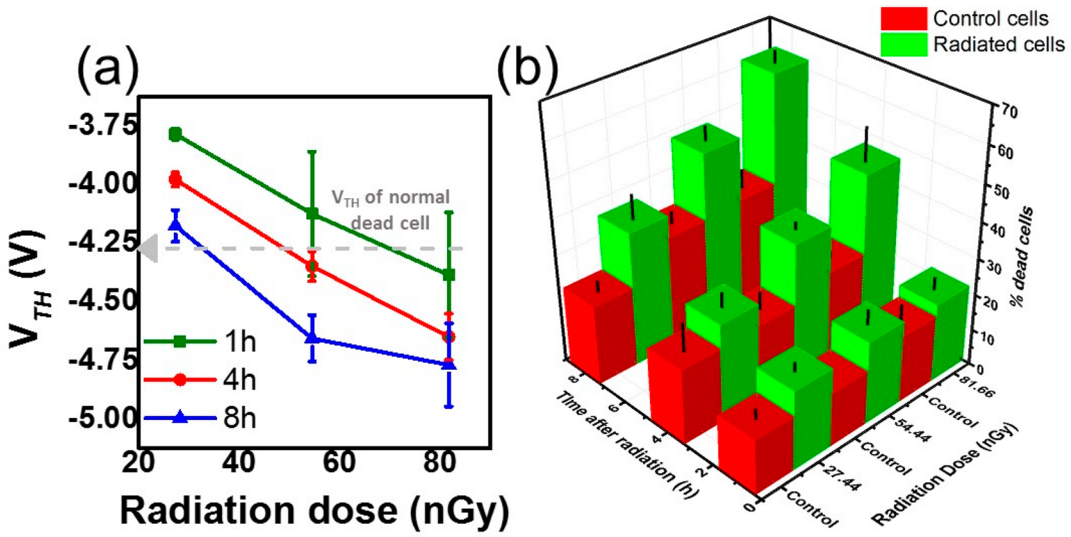

Figure 4. (a) Threshold voltage and radiation dose graph. (b) Hemocytometer count of dead cells %, with dose rate and time after radiation.

apoptosis and the voltage will be constantly monitored to understand the apoptotic pathway mechanism.

Real time measurement of single cell gated transistor (SCGT) transconductance curves is recorded as the gate voltage (V_{GS}) swept from −8 to 0 V and the drain to source voltage (V_{DS}) is held constant at 10 V. The measurements are carried out inside the incubator with 37 °C and 5% CO_2[15] for 8 h (h) for each of the irradiated (apoptotic cells) and control (living cells) samples. The threshold voltage curves of apoptotic cells and normal healthy living cells present clear difference, as shown in Figures S1 and S2a,b. The same threshold voltage measurement is subsequently performed for α-particle irradiated HeLa cell samples with different doses of 27, 54, and 81 nGy. Figure S2c−e shows the change in the threshold voltage curve at different time intervals after irradiation, revealing obvious shift toward negative values with prolonging irradiation time. Furthermore, the real time measurement of the threshold voltage recorded for 8 h signifies the threshold voltage shift between the irradiated and control cell with respect to the doses as shown in Figure 2a−c.

The observed shifts in threshold voltage are the response of n-channel JFET from induced positive charges on single cell gate by the irradiated HeLa cell, which is the combined effect of morphology and ion concentration changes.[12,31] However, as one can see, the threshold slope does not change much while the threshold voltage shifts significantly in Figure S2c−e. This drastic change in the threshold voltage signifies the increase in the ion transfer across the cell as the morphology changes.

During apoptosis, there is an increased activity in potassium ion channels, leading to increase in efflux of potassium ions and consequently shrinking the cell volume which has been well reported.[32] The change in K^+ ion concentration is hypothesized as the reason behind the shift in threshold voltage as a consequence of increased apoptosis-related activities stimulated by irradiation. The results in Figure 2 collectively explains that the increase in the postirradiation time leads to the increase in apoptosis-related activities in the cell.

This change in ion concentration influences the V_{GS} and n-channel width or depth due to a decrease in the depletion layer causing the threshold voltage shift. A mathematical modeling of the threshold voltage with respect to the change in the ion concentration and n-channel width or depth is performed and the results are shown in Figure 3. The finding indicates that the threshold voltage maintains a good linear relation with the ion concentration.[33]

Similarly, in Figure 4a, we observe that increasing the radiation dose leads to shifting of threshold voltages to negative values. From this, it is inferred that increasing dose leads to increase in apoptosis-related activities within the cell. The cell death caused by irradiation are counted using a hemocytometer under microscope and the results are shown in Figure 4b. Over 55−60% of the cells are dead upon irradiation doses of 54 and 81 nGy.

Morphological Apoptotic Changes. HeLa cells in general have a polygonal shape, with the characteristic features of numerous microvilli and lamellipodia extensions, as shown in Figure S3a′−c′. Whereas, the irradiated HeLa cells is observed as spherical in shape with less number of microvilli and small apoptotic bodies present on the cell membrane as shown in Figure 5a′ and g′−i′. In our observation, with increase in the irradiation doses, the change in cell surface morphology is obvious which leads to reduced lifetime of the cell. For the irradiation dose of 54 nGy, the stages of development in apoptotic bodies is clearly visible within 1 h, and a decrease in cell volume is observed after 4 h. At a postirradiation time of 8 h, a significant change in their surface morphology with cell shrinkage and an increased number of dead cells are observed.

These changes were observed to happen faster at the irradiation dose of 81 nGy and finally 8 h postirradiation, the cells shrink, and postapoptosis debris is seen which confirms the cell death process through apoptosis.[29] This is attributed to the release of potassium ions and formation of apoptotic bodies.[30] These changes in cell morphology stages with change in irradiation doses are clearly shown in the Figure 5. α-Particle irradiation induced cell morphology changes with respect to the irradiation dosage and postirradiation time are studied using SEM. The results are shown in Figure 5, while those for the control cells are shown in Figure S3. Together, these results show the real time and in situ response of a single HeLa cell undergoing apoptosis stages under different doses of α-particle irradiation.

DOI: 10.1021/acs.analchem.9b03136
Anal. Chem. 2020, 92, 1738−1745

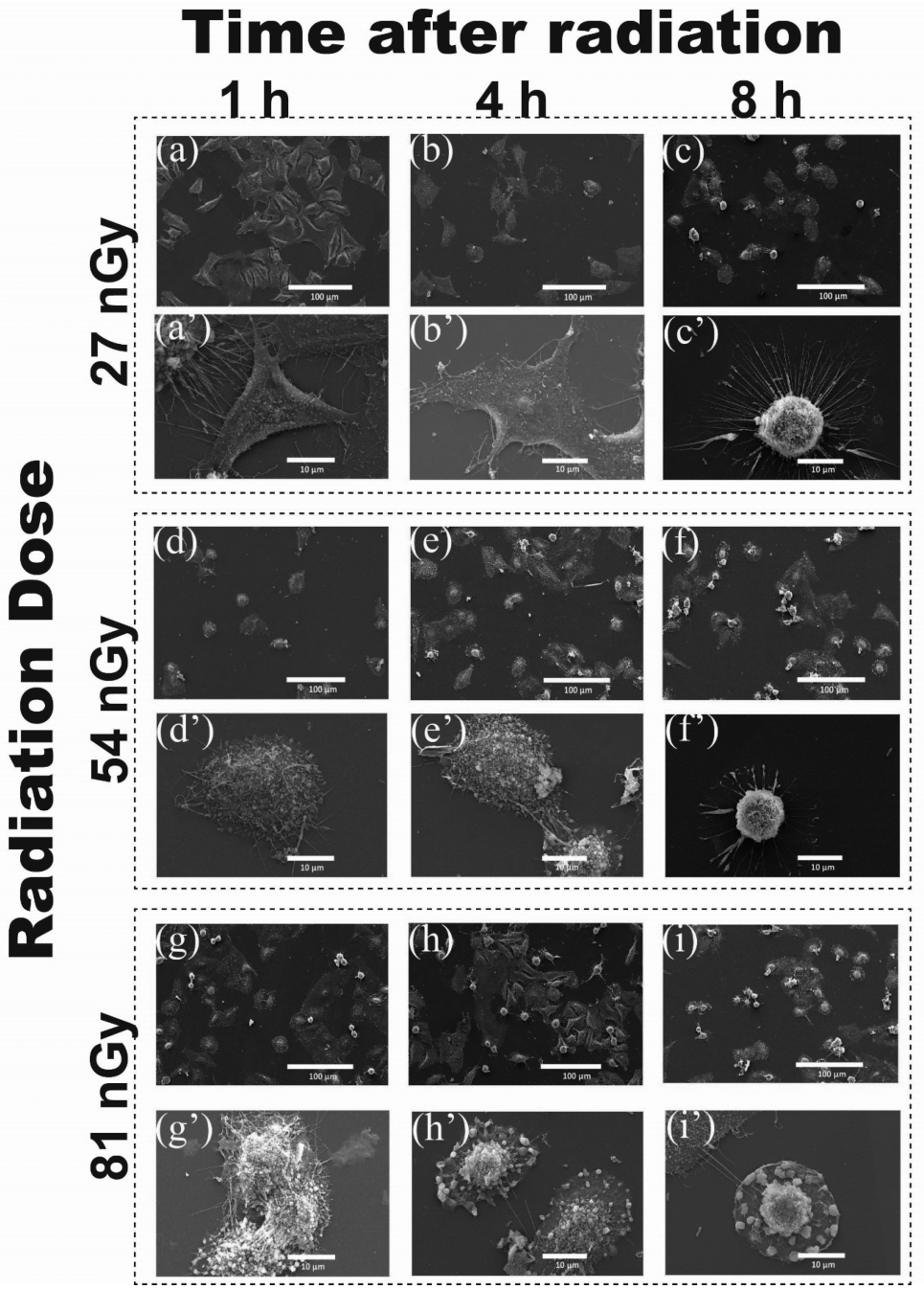

Figure 5. SEM images for irradiated cells: (a,a′) 27 nGy irradiated cells with 1 h postirradiation time, (b,b′) 1 min (27 nGy) irradiated cells 4 h postirradiation time, (c,c′) 27 nGy irradiated cells 8 h postirradiation time, (d,d′) 54 nGy irradiated cells 1 h postirradiation time, (e,e′) 54 nGy irradiated cells 4 h postirradiation time, (f,f′) 54 nGy irradiated cells 8 h postirradiation time, (g,g′) 81 nGy irradiated cells 1 h postirradiation time, (h,h′) 81 nGy irradiated cells 4 h postirradiation time, and (i,i′) 81 nGy irradiated cells 8 h postirradiation time.

The mechanism responsible for threshold voltage shifts is schematically shown in Figure 6. It can be seen in Figure 6a that an exposure of a HeLa cell to α-particle induces damage to its K^+ ion channels in the plasma membrane, thereby resulting in efflux of K^+ ions and depolarization of the cell membrane.[34] To compensate for this depolarization, the Na^+ ion channel opens causing the influx of Na^+ ions into the cell[4,30] (Figure 6b). However, this influx of Na^+ ions is still smaller than the efflux of K^+ ions, ultimately causing the well-known cellular morphological change termed as "apoptotic volume decrease" (AVD).[4,35,36] Due to the increase in the concentration of positively charged ions and formation of apoptotic bodies, the threshold curves show negative shift at postirradiation times of 1 and 4 h, as shown in Figure 6a′,b′. The apoptotic volume greatly decreases after 8 h, thereby increasing the concentration of ions. This progresses into more advanced apoptosis stages and finally results in the formation of apoptotic bodies on the plasma membrane and eventual cell-death[37] (Figure 6c). Again, the threshold voltages shift correspondingly to increase in the concentration of positive ions (Figure 6c′).

The change in the K^+ ion concentration at different postirradiation times were also studied using ICPMS for each irradiation dosage. The increase in the ion concentration level at different post irradiation time infers to the level of

DOI: 10.1021/acs.analchem.9b03136
Anal. Chem. 2020, 92, 1738−1745

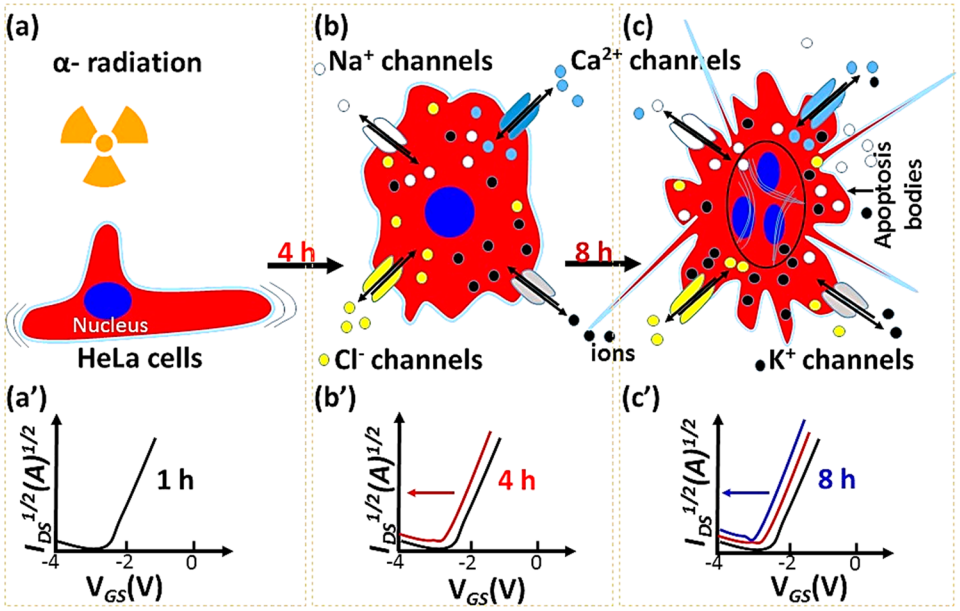

Figure 6. Schematic of mechanism and illustration of threshold voltage shifts due to the ion concentration changes: (a) irradiated HeLa cell and (a′) threshold voltage curve within 1 h; (b) early stage of apoptotic and (b′) threshold curve after 4 h post irradiation time; and (c) formation of apoptotic bodies and threshold voltage shift after 8 h postirradiation time (c′).

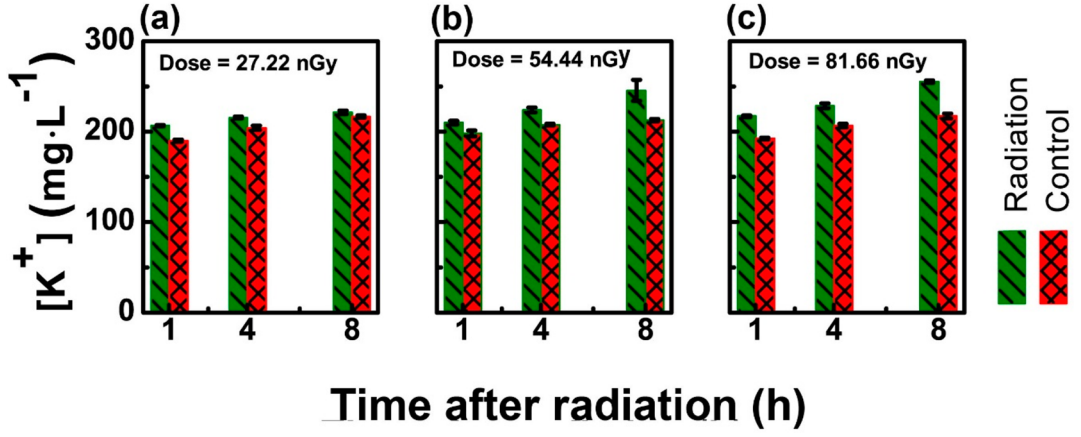

Figure 7. Potassium ion concentration graphs: (a) potassium ion concentration for 27 nGy irradiated cells and their control cells, (b) potassium ion concentration for 54 nGy irradiated cells and their control cells, and (c) potassium ion concentration for 81 nGy irradiated cells and their control cells.

apoptosis. The results from ICPMS analysis shown in Figure 7a–c indicate release of K^+ ion due to the damage of the ion channel after exposure to α-particles, whereas, the concentration of Ca^+ and Cl^- are in very small traces compared to the K^+ ion concentration. These results conclude that K^+ channels play an important role in initiating cell morphological changes and apoptosis-related activities of the cell.[36,38,39] Therefore, the K^+ channel has a role in apoptosis regulation, and it has been proposed as a potential regulator of cancer cell death and a promising anticancer therapy target.[40]

CONCLUSIONS

In this work, we developed a method of using SCGT to monitor the apoptosis process of single HeLa cells induced by α-particle irradiation. We observed that the threshold voltages of the SCGT shift toward negative values, and the magnitude of this shift maintains a good linear relation with the ion concentration and closely associated with the cell morphology change during the apoptosis process. The measurement can be conveniently performed in a cell incubator without needing expensive equipment and labeling agents. With these advantages, we expect that the small dimensions of the nanoneedle combined with the high sensitivity of our SCGT can become a powerful tool for the analysis of single cell responses to various stimuli and facilitate the design of advanced therapies.

ASSOCIATED CONTENT

Supporting Information

The Supporting Information is available free of charge at https://pubs.acs.org/doi/10.1021/acs.analchem.9b03136.

Additional information on electrical control measurements which supports the ion concentration and morphological changes; Figure S1, control measurement for threshold voltages of Hela cells for 1, 2, and 3 min without radiation; Figure S2, threshold voltage measure-

DOI: 10.1021/acs.analchem.9b03136
Anal. Chem. 2020, 92, 1738−1745

ments of living cells, dead cells, and irradiated cells, with the irradiated cells with different doses plotted in parts c−e; and Figure S3, SEM images for the control cells to study the morphologies changes and comparative analysis approved for irradiated cells morphologies (PDF)

AUTHOR INFORMATION

Corresponding Authors

*E-mail:Roy.Vellaisamy@glasgow.ac.uk.
*E-mail: peter.yu@cityu.edu.hk.

ORCID

Xianfeng Chen: 0000-0002-3189-2756
Vellaisamy A. L. Roy: 0000-0003-1432-9950

Notes

The authors declare no competing financial interest.

ACKNOWLEDGMENTS

We would like to acknowledge Mr. Mike Li and Mr. Daniel Yau for providing technical support to conduct the experiments. We acknowledge the grants from RGC of HKSAR Project Number T42-103/16N

REFERENCES

(1) Baslan, T.; Hicks, J. *Nat. Rev. Cancer* **2017**, *17* (9), 557−569.
(2) Liang, S. B.; Fu, L. W. *Biotechnol. Adv.* **2017**, *35* (4), 443−449.
(3) Jin, Z.; El-Deiry, W. S. *Cancer Biol. Ther.* **2005**, *4* (2), 147−171.
(4) Bortner, C. D.; Cidlowski, J. A. *Philos. Trans. R. Soc., B* **2014**, *369* (1638), 20130104.
(5) Svoboda, K.; Yasuda, R. *Neuron* **2006**, *50* (6), 823−839.
(6) Johnson, L. V.; Walsh, M. L.; Bockus, B. J.; Chen, L. B. *J. Cell Biol.* **1981**, *88* (3), 526−535.
(7) Kervrann, C.; Sanchez Sorzano, C. O.; Acton, S. T.; Olivo-Marin, J.-C.; Unser, M. *IEEE J. Sel. Top. Signal Process.* **2016**, *10* (1), 6−30.
(8) Sims, P. J.; Waggoner, A. S.; Wang, C.-H.; Hoffman, J. F. *Biochemistry* **1974**, *13* (16), 3315−3330.
(9) Stephan, G.; Huang, L.; Tang, Y.; Vilotti, S.; Fabbretti, E.; Yu, Y.; Nörenberg, W.; Franke, H.; Gölöncsér, F.; Sperlágh, B. *Nat. Commun.* **2018**, *9* (1), 1354.
(10) Ypey, D. L.; DeFelice, L. J. The Patch-Clamp Technique Explained and Exercised With the Use of Simple Electrical Equivalent Circuits. In *Electrical Properties of Cells*; Plenum Press, 2005; pp 1−55.
(11) Ehrenberg, B.; Montana, V.; Wei, M. D.; Wuskell, J. P.; Loew, L. M. *Biophys. J.* **1988**, *53* (5), 785−794.
(12) Jayant, K.; Porri, T.; Erickson, J. W.; Kan, E. C. Label-Free Electronic Detection of Growth Factor Induced Cellular Chatter on Chemoreceptive Neuron MOS (CvMOS) Transistors. In *TRANSDUCERS 2009−2009 International Solid-State Sensors, Actuators and Microsystems Conference*, Denver , CO, June 21−25, 2009; pp 1814−1817,.
(13) Stern, E.; Steenblock, E. R.; Reed, M. A.; Fahmy, T. M. *Nano Lett.* **2008**, *8*, 3310.
(14) Choi, V. W. Y.; Yum, E. H. W.; Yu, K. N. *Nucl. Instrum. Methods Phys. Res., Sect. A* **2010**, *619* (1−3), 211−215.
(15) Deering, R. A.; Rice, R. *Radiat. Res.* **1962**, *17*, 774−786.
(16) Bernhard, E. J.; Malty, A.; Muschel, R. J. *Radiat Environ Biophys.* **1995**, *34*, 79−83.
(17) Bischof, H.; Rehberg, M.; Stryeck, S.; Artinger, K.; Eroglu, E.; Waldeck-Weiermair, M.; Gottschalk, B.; Rost, R.; Deak, A. T.; Niedrist, T.; et al. *Nat. Commun.* **2017**, *8* (1), 1−11.
(18) Kim, S. Y.; Lee, J.-L.; Kim, K.-B.; Tak, Y.-H. *J. Appl. Phys.* **2004**, *95* (5), 2560−2563.
(19) Lam, E.; Ngo, T. *Manufacturing a PDMS Microfluidic Device via a Silicon Wafer*, MasterHarvard-MIT Division of Health Sciences and Technology HST.410J: Projects in Microscale Engineering for the Life Sciences, Spring 2007, Course Directors Prof. Dennis Freeman, Prof. Martha Gray, and Prof. Alexander Aranyosi, 2007.
(20) Yang, S. H.; Park, J.; Youn, J. R.; Song, Y. S. *Lab Chip* **2018**, *18* (10), 2865.
(21) Adly, N.; Weidlich, S.; Seyock, S.; Brings, F.; Yakushenko, A.; Offenhausser, A.; Wolfrum, B. *npj Flex. Electron* **2018**, *2* (1), 15.
(22) Bart, J.; Tiggelaar, R.; Yang, M.; Schlautmann, S.; Zuilhof, H.; Gardeniers, H. *Lab Chip* **2009**, *9*, 3481−3488.
(23) Hu, X. J.; Liu, H. L.; Jin, Y. X.; Liang, L.; Zhu, D. M.; Zhu, X. Q.; Guo, S. S.; Zhou, F. L.; Yang, Y. *Lab Chip* **2018**, *18*, 3405−3412.
(24) Tan, H.; Guo, S.; Dinh, N. D.; Luo, R.; Jin, L.; Chen, C. H. *Nat. Commun.* **2017**, *8* (1), 663 DOI: 10.1038/s41467-017-00757-4.
(25) Di Carlo, D.; Wu, L. Y.; Lee, L. P. *Lab Chip* **2006**, *6* (11), 1445.
(26) Li, L.; Mak, K. Y.; Shi, J.; Koon, H. K.; Leung, C. H.; Wong, C. M.; Leung, C. W.; Mak, C. S. K.; Chan, N. M. M.; Zhong, W.; Lin, K. W.; Wu, E. X.; Pong, P. W. T. *J. Nanosci. Nanotechnol.* **2012**, *12*, 9010−9017.
(27) Dias-Lopes, G.; Saboia-Vahia, L.; Margotti, E. T.; Fernandes, N. d. S.; Castro, C. L. d. F.; Oliveira Junior, F. O.; Peixoto, J. F.; Britto, C.; Silva Filho, F. C. e; Cuervo, P.; Jesus, J. B. d. *Mem. Inst. Oswaldo Cruz.* **2017**, *112* (10), 664−673.
(28) Wilbur, S.; Yamanaka, M.; Sannac, S. *Characterization of Nanoparticles in Aqueous Samples by ICP-MS*, White Paper, Agilent Technologies, 2015.
(29) Yoon, S.; Park, S. J.; Han, J. H.; Kang, J. H.; Kim, J. H.; Lee, J.; Park, S.; Shin, H. J.; Kim, K.; Yun, M.; et al. *Cell Death Dis.* **2014**, *5* (10), e1494−14.
(30) Kondratskyi, A.; Kondratska, K.; Skryma, R.; Prevarskaya, N. *Biochim. Biophys. Acta, Biomembr.* **2015**, *1848* (10), 2532−2546.
(31) Rane, S. D.; Gore, J. C. *Magn. Reson. Imaging* **2013**, *31* (3), 477−479.
(32) Murakami, T.; Sakata, T.; Matsumoto, A.; Takai, M.; Ishihara, K.; Miyahara, Y. *Trans. Mater. Res. Soc. Jpn.* **2010**, *35* (2), 255−258.
(33) Saha, S. K. *IEEE Access* **2016**, *4*, 507−513.
(34) Kuo, S. S.; Saad, a H.; Koong, a C.; Hahn, G. M.; Giaccia, a J. *Proc. Natl. Acad. Sci. U. S. A.* **1993**, *90* (3), 908−912.
(35) Lang, F.; Hoffmann, E. K. *Compr. Physiol.* **2012**, *2* (3), 2037−2061.
(36) Kondratskyi, A.; Kondratska, K.; Skryma, R.; Prevarskaya, N. *Biochim. Biophys. Acta, Biomembr.* **2015**, *1848* (10), 2532−2546.
(37) Zhang, Y.; Chen, X.; Gueydan, C.; Han, J. *Cell Res.* **2018**, *28* (1), 9−21.
(38) Li, M.; Xiong, Z.-G. *Int. J. Physiol. Pathophysiol. Pharmacol.* **2011**, *3* (2), 156−166.
(39) Huang, X.; Jan, L. Y. *J. Cell Biol.* **2014**, *206* (2), 151−162.
(40) Yu, S. P.; Choi, D. W. *Proc. Natl. Acad. Sci. U. S. A.* **2000**, *97* (17), 9360−9362.

DOI: 10.1021/acs.analchem.9b03136
Anal. Chem. 2020, 92, 1738−1745